

Practical Radio Environment Mapping with Geostatistics

Caleb Phillips, Michael Ton, Douglas Sicker, and Dirk Grunwald

Computer Science Department
University of Colorado
Boulder, Colorado

Email: {caleb.phillips, michael.ton, sicker, grunwald}@colorado.edu

Abstract—In this paper we present results from the first application of robust geostatistical modeling techniques to radio environment and coverage mapping of wireless networks. We perform our analysis of these methods with a case study mapping the coverage of a 2.5 GHz WiMax network at the University of Colorado, Boulder. Drawing from our experiences, we propose several new methods and extensions to basic geostatistical theory that are necessary for use in a radio mapping application. We also derive a set of best practices and discuss potential areas of future work. We find that this approach to radio environment mapping is feasible and produces maps that are more accurate and informative than both explicitly tuned path loss models and basic data fitting approaches.

I. INTRODUCTION

Today, wireless networks are ubiquitous and the importance of their role in our daily lives cannot be underestimated. To a large extent, our ability to build and understand these networks hinges on understanding how wireless signals are attenuated over distance in realistic environments. By predicting the attenuation of a radio signal we can better plan and diagnose networks as well as build futuristic networks that are aware of, and adapt to, the spatiotemporal radio environment. For instance, today's network engineers need methods for accurately mapping the extent of coverage of existing and planned networks, yet the efficacy of those approaches is determined by the predictive power of the underlying path loss model (or interpolation regime). Similarly, researchers that investigate Dynamic Spectrum Access (DSA) networks require accurate Radio Environment Map (REM)s to automate appropriate and timely frequency allocation decisions, yet the performance of these systems is tied intimately to their ability to make meaningful predictions about the current and future occupancy of the radio channel.

Although numerous models have been proposed to predict the vagaries of the radio environment *a priori*, in practice the error associated with these models prevents their use in many applications [1]. The most promising of these models, which involve explicit calculation of diffractions due to obstacles (e.g., [2]), may be more accurate, but have prohibitive data requirements—precise vector models of all three dimensional structures (e.g., buildings and foliage). In the majority of situations where the available environmental data is limited or of low resolution, it is not clear how these models' accuracy is affected, and hence they may not be well enough understood

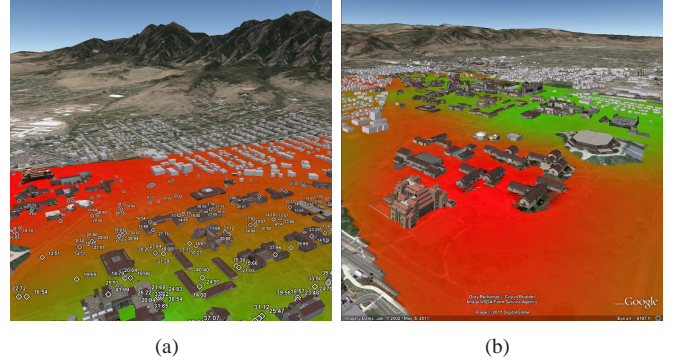


Fig. 1. Examples of coverage map (for CU WiMax cuEN node) overlayed in Google Earth. Green regions indicate strong signal and red regions indicate weak signal.

for practical use in applications that demand high fidelity maps.

The limitations of *a priori* models have led some researchers to an integrated solution that combines some number of careful measurements with predictions (interpolation) (e.g., [3]). And, more recently, some researchers have looked to the promising area of geostatistics as a method of modeling the spatial structure of the radio environment [4], [5]. In this paper, we give a first practical application of geostatistical methods of spatial sampling and interpolation (termed “Kriging” in the geostatistical literature) to the task of mapping the radio environment of a production wireless network. Our approach complements *a priori* modeling, by suggesting a statistically robust method for using measurements to *correct residual error from deterministic models* (e.g., ray-tracing or statistical methods) and common empirical fitting approaches to predicting path loss (e.g., power law fitting). In this way, detailed maps can be generated for both large scale fades, as well as a clear quantification of how small scale fades contribute to the spatial distribution of intrinsic channel variation. We carry out our evaluation using a 2.5 GHz WiMax network operated by the University of Colorado at Boulder. We use our experiences from this case study to develop a set of best-practices for the geostatistical mapping of similar radio environments, and show the real-world abilities of these methods. Figure 1 shows an example of a map produced by our method, overlayed on Google Earth.

In the next section, we will provide some background on geostatistical modeling and on existing work that has proposed

the application of geostatistics to the radio environment mapping problem. In section III, we will describe our approach to geostatistical modeling and interpolation and in section IV we will put these ideas to use in a case study involving mapping the coverage of a set of WiMax base-stations on the University of Colorado campus. Finally, in section V, we will conclude and provide a summary of derived best practices.

II. BACKGROUND AND RELATED WORK

There are a number of fine textbooks that cover the topic geostatistics in depth (e.g., [6], [7], [8]). In this section we aim to provide a brief overview of the relevant background material and prior work.

We claim that the task of practical radio environment mapping can be summarized by five equally important and challenging questions:

- **Sampling:** Where should measurements be made and how many are necessary?
- **Metrics:** What should be measured and how should performance/interference be quantified?
- **Interpolation:** What is the (predicted) value at points that we have not measured?
- **Storage:** How can the resulting maps and models be efficiently stored and queried?
- **Visualization:** How can the stored information be effectively communicated to an end user or network engineer?

A complete solution to the mapping problem must address each of these. In our work here, we have focused on the problems of sampling and interpolation. We have developed modest solutions to the other three problems as well: we use multiple standard, passive metrics in our measurements and propose a method of data combining and visualization that address some of the problems of storage and visualization, but leaves many questions unanswered. Although they are not discussed in detail here, we expect to give a more thorough treatment of these problems in future work. In the remainder of this section, we will provide background on the problems of sampling and interpolation to give context to our approach.

A. Sampling

Choosing an appropriate sampling scheme is application dependent. The shape and variance of the field, as well as domain-specific knowledge about the process being modeled, must be considered when selecting a sampling strategy. Classic spatial sampling schemes can be subdivided into (a) simple random sampling (SRS) where points are selected uniformly at random, (b) systematic (grid-based) sampling designs, (c) stratified, where some regions are sampled more heavily than others, or (d) some hybrid approach marrying systematic, stratified, and random designs.

For the purposes of geostatistical modeling, there are two important criteria that must be considered when selecting an initial sampling design. First, samples must cover the area to be sampled so that no two points are too far apart, which decreases interpolation resolution. Second, some number of samples must be taken at a variety of lags (i.e., the distance

between neighboring measurements) so that relationship between variance and distance can be sufficiently estimated. In particular, clustered measurements are generally required to model small scale effects (i.e., variance from measurements separated by distances smaller than the lag distance). In [9], Olea investigates multiple initial sampling schemes. In his approach, universal Kriging¹ is used to select between several specific designs so that standard error is minimized. Olea strongly endorses stratified random sampling in this work, but it is not clear how well this mechanism works in other domains. In [10], Yfantis et al. study the efficiency of Kriging estimation for various types of sampling lattices. They find that for the majority of cases, where the nugget effect (intrinsic variation) is small relative to the total variance, a triangular grid-based sample is the most efficient initial sampling scheme. The authors suggest that a small pilot sample be used to choose an appropriate density and grid pattern for sampling.

If something is known about the underlying process and its variability, an optimization scheme can be used to select the best initial sample. For instance, in [11], van Groenigan et al., present a framework for Spatial Simulated Annealing (SSA) which uses a fitness function that either spreads points maximally, or chooses their lags according to a prescribed distribution. In SSA, points are varied randomly in a hill-climbing fashion so that an (at least locally) optimal sample is chosen. After the initial sample is chosen, and used to develop an initial model, further refinement can be accomplished with (possibly iterative) “second phase” sampling. There has been some work done in earth sciences [12] and machine learning [13] to determine how additional samples should be selected. In this work we take the approach advocated by Yfantis et al. and perform an initial sample on an equilateral triangular lattice, with some clustered measurements at small random lags. In future work we expect to investigate methods of second phase sampling appropriate for this domain

A final important question for scalability is whether some or all of these samples can be collected automatically, perhaps by users of the network being studied itself (“crowd sourcing”). Although there have been some recent developments in the area of crowd-sourced network measurement (e.g., [14]), it is not clear whether commodity devices are able to collect measurements with sufficient fidelity to be of use for REM applications. Although mobility models may offer some hints, it is also not clear whether users visit the locations where measurements are needed most, or whether the stochastic temporal nature of crowd-sourced measurements affect model precision. In future work we hope to study the practical limitations of crowd-sourced sampling, and determine whether this approach can be used to scale empirical REM data collection to large (country-sized, perhaps) areas.

B. Interpolation

The problem of interpolation is at the center of any measurement based approach to radio environment mapping. Interpola-

¹Universal Kriging (UK) and Ordinary Kriging (OK) are interpolation techniques used in geostatistics. They will be discussed in more depth below.

tion attempts to use some number of measurements to predict the value at points that have not been measured. One solution, from the field of geostatistics, is known as Kriging after the seminal work of Dain Krige on mine valuation in the 1950's and 60's. As compared to alternative methods of interpolative mapping, such as Inverse Distance Weighting (IDW), Kriging has three important benefits: (1) it is preceded by an analysis of the spatial structure of the data and an estimate of the average spatial variability of the data is integrated into the interpolation process via the variogram model, (2) it is an exact interpolation method meaning that when data is available at a given point, the interpolated map has exactly that measured value at that point, and (3) since it is a robust statistical method, it provides a per-prediction indication of estimation standard error via the square root of the Kriging variance [7].

There have been several papers that have attempted to develop interpolation strategies appropriate for wireless coverage mapping. In [15], Connelly *et al.* suggest a way to interpolate between Received Signal Strength (RSS) measurements using IDW and claim less than 1 dB interpolation error. Although promising, this work makes strong simplifying assumptions (for instance, assuming propagation stops after 100 m), which prohibit use in the applications we are considering here. In [16], Dall'Anese suggests a way to use distributed measurements from sensors to determine a sparsity promoting Weighted Least Squares (WLS) interpolated coverage map. The authors assume that the location of sensors is not controllable and that the principle application is in empirically determining a safe transmit power for a given radio so as to avoid interfering with primary users (PUs). In [4], Konak proposes the use of Ordinary Kriging (OK) over grid-sampled data for mapping coverage and shows that this approach can outperform a neural network trained model presented in [17]. Finally, [18] provides a tutorial addressing the use of basic geostatistical interpolation for estimating radio-electric exposure levels. While not strictly the same as wireless network propagation, the approach is relevant.

In addition to these works, there have been several recent publications by Riihijärvi *et al.* that discuss the use of spatial statistics to model radio propagation [19], [5]. Like [4], this work presumes a sampling on a regular rectangular grid. Measurements are used to fit a semivariogram and several underlying functions are investigated. In [20], the authors suggest how this method can be used to more compactly store radio environment maps and in [21] the authors investigate how the placement of transmitters, terrain roughness, and assumed path loss effects the efficacy of the interpolated field. In this paper, we build upon the foundational work of Riihijärvi and Konak by making an empirical evaluation of these geostatistical techniques, applying them to the general case of coverage mapping, and evaluating them in a realistic environment.

III. METHOD

If we assume that there is a random field that we are modeling called Z , then the value of that field at a point in space \mathbf{x} is $Z(\mathbf{x})$. The field can be defined in any dimension, but typically we would assume that $\mathbf{x} \in \mathbb{R}^n$ with $n = 2$ or $n = 3$. We can then define the value at any point as the field mean (μ) plus some error ($\epsilon(\mathbf{x})$):

$$Z(\mathbf{x}) = \mu + \epsilon(\mathbf{x}) \quad (1)$$

This model, which is used in Ordinary Kriging (OK), assumes a constant (stationary) mean in space. Generalizations that drop this assumption allow for nonlinear constructions and are generally termed Universal Kriging (UK), but are likely overpowered for this application. As we will show below, OK methods are sufficiently powerful if care is taken to remove trend (bias) from the process prior to modeling.

A. The Variogram

Central to geostatistics is the variogram, a function that models the variance between two points in space as a function of the distance between them (\mathbf{h}). In the case of grid-sampled fields, the distance between measurements is a fixed lag distance. Randomized and optimized sampling schemes produce variable lag distances. The theoretical variogram is typically written as:

$$\gamma(\mathbf{h}) = \frac{1}{2} E[(Z(\mathbf{x} + \mathbf{h}) - Z(\mathbf{x}))^2] \quad (2)$$

If we know that the field is second order stationary (i.e., a measurement at the same point will not vary with time, and the difference between two measurements is also constant with time), then the covariance function (correlleogram) is defined as:

$$C(\mathbf{h}) = E[(Z(\mathbf{x}) - \mu)(Z(\mathbf{x} + \mathbf{h}) - \mu)] = C(\mathbf{0}) - \gamma(\mathbf{h}) \quad (3)$$

The assumption of second order stationarity may not be safe for many radio environments, especially those operating at low frequencies. Extending our work here to incorporate nonstationary models is an exciting area for future work that is outside of the scope at present.

If we have some set of measurements, we can define an empirical variogram:

$$\gamma'(\mathbf{h}_i) = \frac{1}{2n} \sum_{j=1}^n (Z(\mathbf{x}_j + \mathbf{h}_i) - Z(\mathbf{x}_j))^2 \quad (4)$$

A typical problem is to fit a variogram model (or correlleogram) to an empirical variogram curve, given some number of measurements. There are a number of models that can be used for fitting. One example is the exponential model:

$$\gamma_{exp}(\mathbf{h}) = \tau^2 + \sigma^2(1 - e^{-h/\phi}) \quad (5)$$

In this equation, τ^2 is known as the nugget variance and is used to model discontinuity around the origin. In radio,

this would correspond to the intrinsic variation (small scale fading) of the channel. σ^2 is known as the sill because it sets the maximum value (variance) of the semivariogram. Larger values of σ will increase the level at which the curve flattens out. Finally, the parameter ϕ acts as a scale and affects the overall shape of the curve. The value of ϕ determines the rate at which variance is expected to appear as a function of distance (lag) between points. There are a number of other models, such as the Gaussian, Cauchy, and Matérn models, which may or may not be the best fit depending on the data². As we will see for the networks and metrics we study here, the classical Gaussian and Cubic models perform well. In this work we perform variogram fitting using the weighted least squares (WLS) method described in [23], using the implementation available in the R package “geoR” [24]. In our implementation, variogram fitting is automated by fitting multiple functions and parameter combinations and choosing the best fit via cross validation. Although computationally intense, this fitting process can be trivially parallelized so that it can be accomplished quickly. For instance, by computing and cross-validating fits in parallel. Data-parallelism can also be achieved by fitting measurements from each transmitter separately, in parallel.

B. Kriging

OK is an interpolation technique that predicts the unknown value at a new location ($Z(\mathbf{x}')$) from the weighted known values at neighboring locations (\mathbf{x}_i):

$$Z_K(\mathbf{x}') = \sum_{i=0}^n w_i Z(\mathbf{x}_i) \quad (6)$$

To determine the optimal weights (\mathbf{w}), we must minimize the estimation variance σ_E^2 :

$$\sigma_E^2 = E[(Z_k(\mathbf{x}') - Z(\mathbf{x}')^2] \quad (7)$$

where

$$\sigma_E^2 = -\gamma(\mathbf{x}' - \mathbf{x}') - \sum_{i=1}^n \sum_{j=1}^n w_i w_j \gamma(\mathbf{x}_i - \mathbf{x}_j) + 2 \sum_{i=1}^n w_i \gamma(\mathbf{x}_i - \mathbf{x}') \quad (8)$$

which leads to the system of equations:

$$\begin{pmatrix} \gamma(\mathbf{x}_1 - \mathbf{x}_1) & \dots & \gamma(\mathbf{x}_1 - \mathbf{x}_n) & 1 \\ \vdots & \ddots & \vdots & \vdots \\ \gamma(\mathbf{x}_n - \mathbf{x}_1) & \dots & \gamma(\mathbf{x}_n - \mathbf{x}_n) & 1 \\ 1 & \dots & 1 & 0 \end{pmatrix} \begin{pmatrix} w_1 \\ \vdots \\ w_n \\ \mu \end{pmatrix} = \begin{pmatrix} \gamma(\mathbf{x}_1 - \mathbf{x}_0) \\ \vdots \\ \gamma(\mathbf{x}_n - \mathbf{x}_0) \\ 1 \end{pmatrix} \quad (9)$$

²[22] provides an excellent survey of these models.

where μ is called the Lagrange parameter. This interpolation is “exact”, meaning that $Z_K(\mathbf{x}') = Z(\mathbf{x})$ if $\mathbf{x} = \mathbf{x}'$. This approach can be used for mapping by Kriging the value at each pixel position. In this application, the system in equation 9 is solved for each unknown pixel value (\mathbf{x}'). This constitutes a substantial amount of work, but is trivially parallelizable (e.g., by performing each pixel calculation simultaneously).

The quality of an interpolated field depends on the goodness of the fitted variogram (γ). In addition to this, there are a number of different ways to adapt Kriging to a specific data set. Anisotropic corrections are of particular interest for coverage mapping. This approach assumes that the field may require different statistics (i.e., a different variogram and possibly fitting method) in different directions from some point. There is also an entire branch of statistics dealing with multivariate analysis (co-Kriging).

C. Detrending

In [22], Olea et al describe the importance of removing any sources of nonlinear trend from measurements so that the fitted (interpolated) field complies with the basic tenets of geostatistics. To this end, we introduce a hybrid approach where a predictive (empirical) model is used to calculate the predicted path loss value at each measurement point. This approach differs from the direct fitting method suggested by Riihijärvi and Konak. In our method, the model prediction is subtracted from the observed value to obtain the residual, or error:

$$Z'(\mathbf{x}) = Z(\mathbf{x}) - P(\mathbf{x}) \quad (10)$$

where $Z'()$ is the residual (de-trended measurements) process, $Z()$ is the observed process and $P()$ is the model prediction. This approach to detrending is entirely modular and extensible— $P()$ can be replaced with any predictive model. In this way, the geostatistical interpolation can be viewed as a careful way to correct for any remaining (environment specific) model error, instead of as a complete replacement. And, as the state of the art in path loss modeling is advanced further, and models are able to make predictions closer to measurements, this improvement can be carried through to measurement-based interpolation in the process of de-trending as described here.

In our work here, we detrend signal strength measurements with a fitted model for path loss from [1]. First, we convert the measurements from signal power/ratio (i.e., Carrier to Interference and Noise Ratio (CINR)), to path loss. This requires some basic knowledge about the transmitter: transmit power (P_{tx} in dBm), antenna gain in the direction of the receiver ($G_{tx}(\theta)$ in dB), and an assumed constant noise floor value (N in dBm, set to -95 here).

$$Z_{pl}(\mathbf{x}) = (P_{tx} + G_{tx}(\theta)) - N - Z_{cinr}(\mathbf{x}) \quad (11)$$

If this information is not known, approximate values can be substituted which will be corrected automatically in the

fitting process, and should have no discernable ill-effect on the accuracy of the interpolation.

Using the observations from each transmitter, we fit the parameters α (path loss exponent) and ϵ (offset) in the following equation:

$$P(\mathbf{x}) = \alpha 10 \log_{10}(d) + 20 \log_{10}(f) + 32.45 + \epsilon \quad (12)$$

where d is the distance from the point \mathbf{x} to the transmitter in km and f is the frequency of the transmission in MHz. Subtracting the fitted value of $P()$ for from each measurement gives the de-trended observations ($Z'(\mathbf{x})$), which can then be used to fit an empirical variogram model.

D. Summary of Complete Method

In summary, the complete mapping process is as follows: We begin by determining the extent of the area of interest, and defining a bounding box for measurements (and prediction). Following the best practices for geostatistical sampling described in section II-A, a uniform (equilateral triangular) sample grid is generated and used for the initial sampling. Some small number of pilot measurements may be necessary to determine an appropriate lag distance (sampling density) for this grid.

Next, measurements are taken at the grid points. At a subset of grid locations, random clustered measurements are also taken within 40 wavelengths (4.8 m) of the original point. When the resulting data from the initial sample is available, it must be inspected for sources of systematic bias and measurement error. Sources of measurement error may differ from campaign to campaign, but are generally systematic (i.e., equipment or procedural error) or spatial (i.e., sources of error or interference stemming from the position of the measurement apparatus relative to its surroundings). When bias is suspected in the measurements, these issues must be approached on a case-by-case basis.

Next, using the method described in section III-C, we detrend the measurements. The detrended measurements are then used to generate an empirical variogram, and theoretical variogram fit as described in section III-A. Using the variogram and measurements, a WLS OK method can be used to interpolate the values at each pixel location. We recommend 0.2 pixels per meter for high resolution maps, and 0.05 pixels per meter for low resolution (prototyping) maps.

The OK process produces a map with an interpolated value and error (Kriging variance) at each pixel location. This step requires substantial computation (especially at high resolutions). Optionally, second-phase samples can be taken to fine tune the model and reduce residual error further. After each round of additional sampling, the variogram fitting and Kriging steps must be repeated. Finally, the trend is added back to pixel values to produce a final raster image.

IV. CASE STUDY: WiMAX

In this section, we describe a case study conducted specifically for the purpose of evaluating the efficacy of Kriging-based coverage mapping. Our aim here is to map the coverage

| Name | Dir. | Freq. | Longitude | Latitude | AGL (m) |
|------|------|-------|-------------|-----------|---------|
| cuGW | 235 | 2530 | -105.267778 | 40.008056 | 46 |
| cuGE | 90 | 2520 | -105.267778 | 40.008056 | 46 |
| cuEE | 120 | 2530 | -105.263056 | 40.007222 | 34 |
| cuEW | 240 | 2510 | -105.263333 | 40.007222 | 34 |
| cuEN | 0 | 2578 | -105.263333 | 40.007222 | 34 |

TABLE I
SPECIFICATIONS OF FOUR UNIVERSITY OF COLORADO WiMAX BSs.



Fig. 2. Map of University of Colorado and 100m uniform equilateral triangular sample. Measurements are limited to the main campus, which is outlined in red.

of five WiMax base-stations deployed on the University of Colorado at Boulder campus operating at 2.5 GHz within an educational spectrum license held by the University. Although this study seeks to map the coverage of this network, the problem is analogous to passively mapping the coverage of a Primary User (PU) or an interfering (possibly rogue) transmitter.

To determine an appropriate sampling density, we prototyped our methods on publicly available data, collected from a municipal wireless network in Portland, Oregon operating at a similar frequency (2.4 GHz) [25]. Based on this pilot study we chose to perform an initial sample on a uniform equilateral triangular lattice, following the recommendation of [10], with a lag of 100 m. To constrain the data collection, we confine measurements to the main University of Colorado campus. Figure 2 shows the main campus along with points at which we aimed to collect samples. The shape of the University is vaguely triangular, with the longest side measuring 1.5 km and the shorter side measuring 1.1 km, giving a total measurement area of slightly more than $825m^2$.

Of the five WiMax Base Station (BS)s being studied, four are managed by the University of Colorado Office of Information and Technology (OIT) and primarily provide backhaul coverage to buses in and around Boulder. The fifth is a Global Environment for Networking Innovation (GENI) testbed node

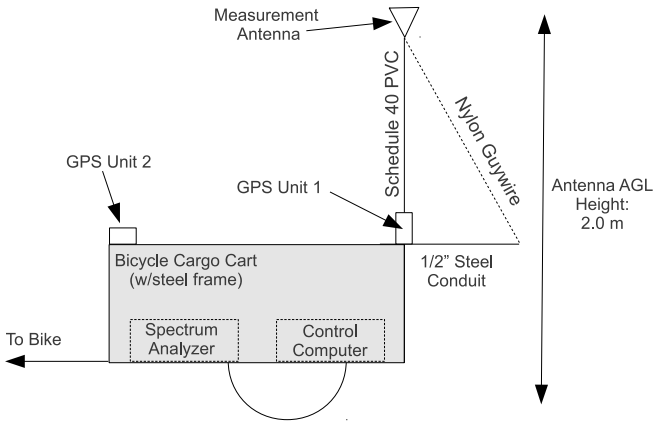


Fig. 3. Diagram of WiMax measurement cart.

meant for research purposes [26]. Table I provides details about the location and configuration of each BS³. All nodes use a channel bandwidth of 10 MHz, have 90-degree sector antenna (excepting the GENI node which has a 120 degree sector), and operate at a nominal transmit power of 40 dBm. Two BSs are deployed on the Gamow Physics Tower (pointing east (cuGE) and west (cuGW)) and three on the Engineering Center tower (pointing north (cuEN), east (cuEE), and west (cuEW)).

A. Measurement Apparatus and Procedure

In order to make measurements in arbitrary locations, which might not be accessible with a large vehicle, we constructed a measurement apparatus of our own design, built into a small cart. The cart provides a stable platform on two wheels and can be connected to a bicycle or used as a hand-cart. Figure 3 shows the design and layout of the measurement cart. To collect measurements, we make use of an Anritsu MS2721B portable spectrum analyzer. This analyzer is unique in that it is both battery-powered and portable, as well as having the ability to demodulate WiMax transmissions and record protocol-specific quality metrics. To control the spectrum analyzer, we use the Virtual Instrument Software Architecture (VISA) National Instruments (NI) interface. A small netbook laptop running Ubuntu Linux is connected to the spectrum analyzer with a single Category 5 (CAT5) crossover cable. This laptop controls the spectrum analyzer using a series of VISA commands, which allows for measurement scripting on the laptop. Two Global Positioning System (GPS) devices are used to record position, one connected to the spectrum analyzer and one a hand-held Garmin GPS60 device⁴. The measurement antenna for the spectrum analyzer is raised 2 m from the ground using a piece of schedule-40 Polyvinyl Chloride (PVC) (non-conductive) pipe, and attached with plastic cable ties. Although the cart itself is conducting, care is

³Unless otherwise specified, all latitude and longitude coordinates are given in WGS84/EPSC:4326 and UTM coordinates in EPSG:32160.

⁴We chose to use a hand-held GPS device after finding the Anritsu's GPS support to be very unreliable.

made to ensure that no metallic objects are in close proximity to the elevated measurement antenna.

We chose to focus our measurement effort on four important first order metrics of channel performance that can be collected passively: CINR, Relative Constellation Error (RCE), Error Vector Magnitude (EVM), and subcarrier spectrum flatness. CINR provides a measurement of pure received power above noise, calculated from a clean carrier wave transmitted in the preamble of the WiMax frames. RCE and EVM quantify the amount of error in a binary or quaternary constellation plot, which provides a tight estimate of physical-layer error. Finally, subcarrier spectrum flatness is the amount of gain or attenuation on each of 52 (or more) subcarriers within the bandwidth relative to the mean signal strength. Using the spectrum flatness data, we are able to calculate Effective Signal to Noise Ratio (ESNR), the metric shown in [27] to be a strong predictor of actual network performance (as compared to the more traditional metrics such as Signal to Noise Ratio (SNR) and RSS). We verified this result for WiMax networks by performing upstream and downstream throughput tests to the Access Service Network (ASN) gateway at a random (spatial) sample of points—both ESNR and CINR appear to be reasonable physical layer predictors of application layer performance. ESNR can be thought of the average SNR required to produce the error process seen on each individual subcarrier. In this paper we use the label “ESNR6” to refer to the ESNR metric using the modulation used at 6 Mbps (i.e., QPSK), and “ESNR54” for the ESNR metric using the 54 Mbps modulation (i.e., QAM). Although we have used sensitive measurement equipment to ensure accuracy in this study, recent work using commodity devices (e.g., [28], [29]), suggest that future systems may be largely implemented with inexpensive and easily obtainable hardware, which may already be available in some end-user mobile devices.

Before we begin measurement, we must define a policy for locating and measuring at sample sites. After some experimentation with direct location using a GPS device, we settled on a simple solution involving a printed map similar to the map in figure 2. We visit each site without any particular order. In the event that it is impossible to make a measurement at the site, either because it falls in an inaccessible (i.e., fenced) area or within a building, we instead measure the closest point (by straight line distance) that is accessible. Although there is some random error associated with locating points (due to GPS accuracy, point finding, and obstacles), we claim that this error is not harmfully aligned with any environmental feature and instead amounts to random jitter about the uniformly selected sample sites (which some spatial sampling studies have actually purposely advocated).

At each measurement location, a wireless keyboard⁵ is used to manage the control computer (which keeps the experimenter away from the apparatus, preventing them from interfering with the measurements themselves) and the control computer

⁵The keyboard operates in the 2.4 GHz spectrum, and hence will not interfere with our measurements around 2.5 GHz.

provides feedback through an amplified speaker utilizing text-to-speech synthesis software. At each point, three repeated measurements are made of downstream system performance using the various metrics. At a subset of points, additional clustered measurements were taken within a 40 wavelength (≈ 4.8 m) radius of each true point. The combination of repeating measurements in time and space, allows for accurate estimation and averaging of intrinsic channel variability due to small scale fading effects and instrument error.

The device first picks a given channel (carrier frequency) and then records all metrics for each measurement in turn. Then it switches to a different channel and repeats. While the device is performing measurements, the experimenter uses the handheld GPS device to record the current position, sample location (each sample site is assigned a unique identifier), and GPS accuracy. At the end of a measurement effort (typically when the analyzer's battery is flat), the cart is returned to the laboratory for charging and data offload. The spectrum analyzer stores measurements in a proprietary, but plain/text, format that can be easily parsed.

B. Possible Sources of Systematic Sampling Error

During our measurement campaign, three individuals used the cart to make measurements. Although all three measurers were collecting measurements using the same procedure, one possible source of systematic error is from the measurers themselves. No significant correlation is present in terms of location error or measurement variation and hence we do not correct for this bias in subsequent analysis. It is worth noting that some measurements are distant from their intended location. This occurs (as discussed above), when a point is unreachable. So long as the new measurement point is as close to the original measurement location as possible and there is no systematic error or systematic terrain alignment, these deviations should not effect the quality of the sample. We also investigated the relationship between GPS accuracy and channel variation, hypothesizing that GPS accuracy might be weaker in complex environments where signal is also degraded, but no discernible correlation was present.

C. Correlation Between Metrics

In this measurement campaign, we collected several performance metrics besides the classic signal strength or SNR-equivalent metrics. One question that naturally arises is: are these more robust metrics trivially correlated with simple and easy to collect metrics such as CINR. Figure 4 plots the relationship between CINR and each of the other metrics studied. RCE and EVM appear to be a simple (but nonlinear) function of CINR, at least as calculated by the spectrum analyzer used in this study. There are several ways that EVM can be calculated from the constellation plot and observed power of constellation points. It appears that the Anritsu spectrum analyzer is calculating EVM from CINR or vice versa. RCE is calculated directly from the EVM value and hence is equivalent. Given this, RCE and EVM do not appear to provide novel information above and beyond what

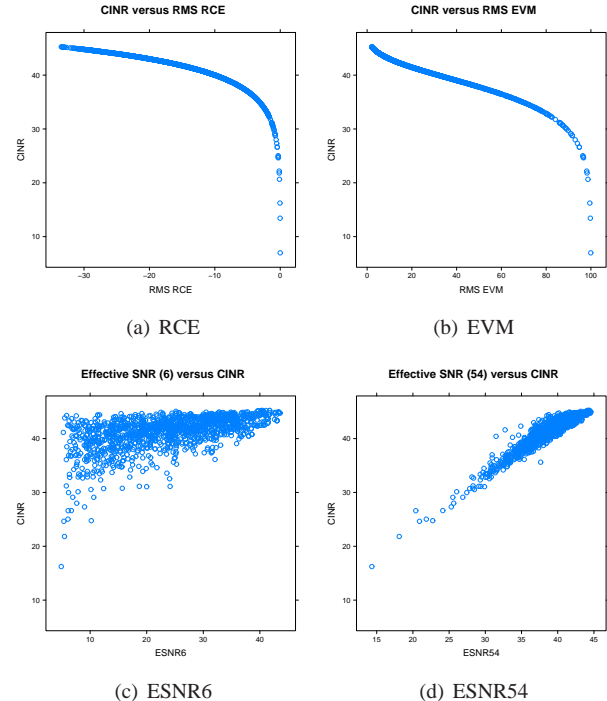


Fig. 4. Correlation between metrics and CINR.

is provided by the CINR measurement. It is worth noting that in the process of data collection, we have recorded a complete constellation plot for each measurement so we could also calculate RCE ourselves. The relationship between ESNR and CINR is less trivial, especially for the lower (Phase Shift Keying (PSK) modulation based) bitrates. The higher bitrates, which use Quadrature Amplitude Modulation (QAM), tend to have a fairly well defined linear correlation with CINR. A least squares fit of ESNR54 to CINR is very good with adjusted R^2 of 0.90 and mean residual error of 1.01 (as compared with 0.29 R^2 and 8 dB residual error for ESNR6). This suggests that in cases where information about spectrum flatness is unavailable, ESNR54 can be roughly approximated using CINR measurements.

D. Spatial Data Characterization and Variogram Fitting

Figure 6 shows CINR measurements taken for the “cuEN” BS. By plotting the measurements in this way, we can identify any sources of skew and bias in the measurements, as well as understand their distributional spread and variance prior to geostatistical modeling. All four metrics produce a similar spatial distribution of values with large path loss or error values to the southwest and smaller (better) values to the north. All metrics have different value distributions, but the ESNR54 and CINR metrics appear to share the same basic skewed lognormal shape. Figure 5 shows the fitted relationship between path loss and distance for the three SNR-like metrics. The fits are poor, but appear to at least account for some basic trend, which we can remove to improve the efficacy of the Kriging process. At locations where we attempt, but fail, to make a measurement, we use a noise-floor value. We call these “null measurements”. For the SNR-like metrics, we use 1.0

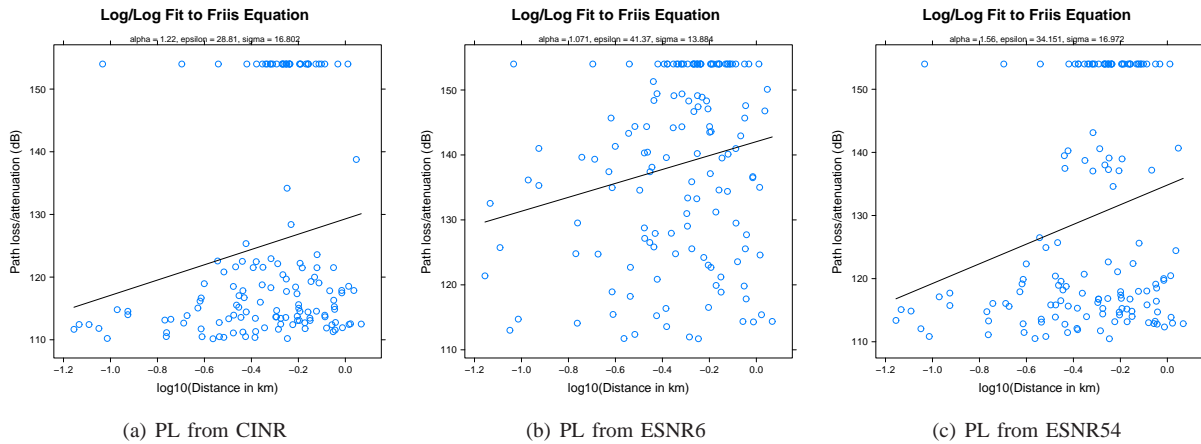


Fig. 5. De-trending fits for the CU WiMax cuEN (GENI) node. Only the metrics that can be converted to path loss and de-trended (i.e., SNR and equivalents) are shown.

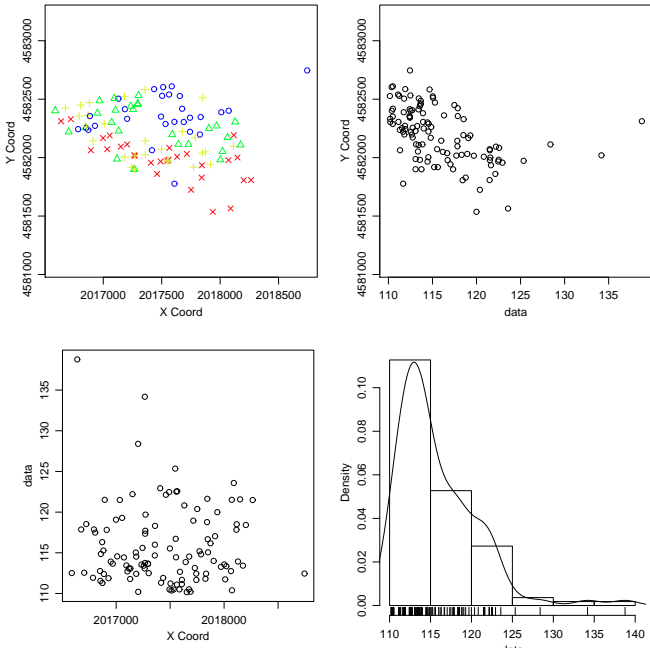


Fig. 6. Measurement spatial structure for CU WiMax cuEN (GENI) CINR measurements.

and for EVM, we use 100 (i.e., 100% probability of error) as the null measurement value.

After detrending and accounting for null measurements, we can proceed with variogram fitting. Figure 7, shows the fitted variograms for cuEN. The fits are truncated at 1 km here, since this is approximately the diameter of the measurement region, and measurements further apart than that are unlikely (or erroneous). Because we have attempted to model the nugget variance explicitly with clustered measurements, we can set the nugget tolerance to zero⁶. The fitted variogram parameters are summarized in table II.

In this data set, the best fits are generally truncated, but without inclusion of null measurements. This differs from our pilot study with the data at [25], but makes sense given that the sampling has been carried out in a consistent way here, which perhaps is able to model the decay of the signal towards the noise floor without including “implicit” measurements. The best fits are split fairly evenly between Gaussian and cubic models, with a slight preference for Gaussian.

The goodness of these nonlinear fits is determined via experimental cross validation. We randomly exclude 20% of points, and use the remaining points to predict the value of each excluded point. This results in root mean square error (RMSE) and mean square-root of kriging variance (MSKV, i.e., model standard error) reported the table. We can see that the quality of fit is clearly correlated with the metric used—CINR fits much more cleanly than the ESNR metrics. The CINR fits result in a residual standard error of 2-4 dB depending on the AP being modeled, which is quite good by the standard of *a priori* models [1]. The worst fits, for the ESNR metrics, produce 9-10 dB residual error, which is on the same scale as *data-fitted* path loss models. To highlight this improvement, a final column in this table provides the gain achieved in terms of dB RMSE over a simple data-fitting method. Why the ESNR metrics appear to be more difficult to fit is an open question. However, it may be due to the fact that ENSR involves discrete steps (and more degrees of freedom) whereas CINR is a single continuous variable. In addition to standard error, we have also calculated the gain (reduction in error) versus an explicit log/log fit to the measurements. We can see that the geostatistical fitting method produces a modest reduction in residual error for all metrics and all BSs. Although the gain over an explicit log/log fit is small, this is encouraging since the geostatistical model has more degrees of freedom and includes knowledge of spatial structure.

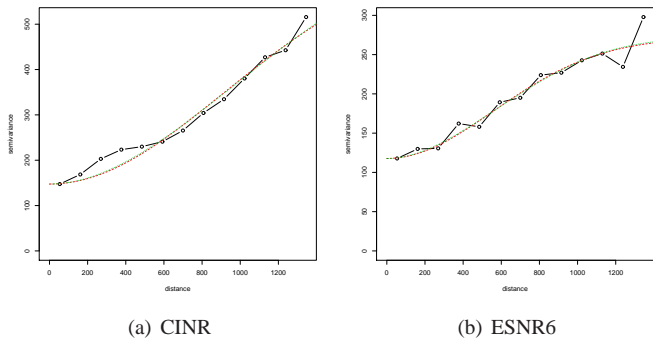
E. Mapping with Ordinary Kriging

Mapping proceeds by Kriging each pixel in the prediction region and then creating a color map by interpolating the

⁶Nugget tolerance is the distance within which measurements are considered to be effectively colocated.

| BS | Metric | Model | ϕ | τ^2 | σ^2 | N | Trunc/Neg | Mean K-Var | Mean RMSE | Gain |
|-----------|--------|----------|---------|----------|------------|-----|-------------|------------|-----------|-------|
| cuEW | EVM | gaussian | 697.13 | 199.12 | 351.34 | 150 | FALSE/FALSE | 15.00 | 16.05 | N/A |
| cuEW | CINR | cubic | 1839.69 | 3.99 | 19.38 | 150 | FALSE/FALSE | 2.16 | 2.75 | 17.54 |
| cuEE/cuGW | ESNR54 | cubic | 2183.29 | 115.19 | 81.75 | 147 | TRUE/FALSE | 11.09 | 9.27 | 5.88 |
| cuEE/cuGW | ESNR6 | cubic | 1253.62 | 91.27 | 45.66 | 147 | FALSE/FALSE | 9.95 | 9.50 | 2.68 |
| cuEE/cuGW | EVM | cubic | 771.36 | 259.17 | 396.46 | 147 | TRUE/FALSE | 17.68 | 15.91 | N/A |
| cuEE/cuGW | CINR | gaussian | 541.94 | 8.48 | 9.30 | 147 | TRUE/FALSE | 3.04 | 2.87 | 12.65 |
| cuGE | ESNR54 | gaussian | 2340.33 | 34.11 | 437.08 | 182 | TRUE/FALSE | 5.93 | 6.91 | 7.15 |
| cuGE | ESNR6 | gaussian | 380.27 | 49.67 | 39.18 | 182 | TRUE/FALSE | 7.34 | 7.48 | 2.99 |
| cuGE | EVM | gaussian | 310.67 | 138.75 | 321.18 | 182 | TRUE/FALSE | 12.67 | 12.25 | N/A |
| cuGE | CINR | cubic | 1711.76 | 6.39 | 12.31 | 182 | FALSE/FALSE | 2.61 | 2.03 | 9.80 |
| cuEN | ESNR54 | cubic | 1530.11 | 72.81 | 108.83 | 146 | TRUE/FALSE | 9.00 | 9.83 | 7.97 |
| cuEN | ESNR6 | gaussian | 746.71 | 118.74 | 76.04 | 146 | TRUE/FALSE | 11.22 | 11.21 | 2.67 |
| cuEN | EVM | cubic | 751.21 | 444.98 | 357.14 | 146 | FALSE/FALSE | 22.84 | 21.11 | N/A |
| cuEN | CINR | cubic | 1304.05 | 14.22 | 20.04 | 146 | TRUE/FALSE | 4.00 | 4.09 | 12.80 |

TABLE II
BEST FIT STATISTICS FOR VARIOGRAM FITTING OF CU WiMAX BSs.

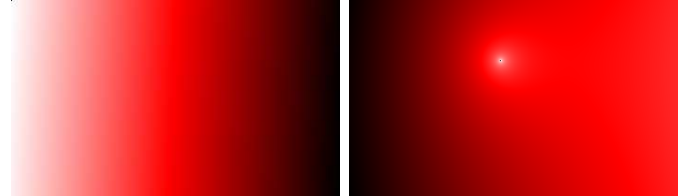


(a) CINR

(b) ESNR6

(c) ESNR54

(d) EVM



(a) CINR, Excess

(b) CINR, Map

(c) ESNR6, Excess

(d) ESNR6, Map

(e) ESNR54, Excess

(f) ESNR54, Map

Fig. 7. Empirical variogram and fits of four metrics for CU WiMax cuEN (GENI) node.

kriged value on a color gradient. This color mapping scheme was adapted from medical imaging [30] and appears to work well for visualizing the radio environment. Figure 8 shows the final maps for the cuGE node, which features an interesting final propagation pattern. This BS is a 90-degree sector pointing east, and as a result the propagation seems to favor that direction, however, there are clear and significant shadows to the west and north.

As a final metric of performance for these maps, each map is compared to a random sample of measurements taken around campus to see how well the maps are able to predict points *in between* the sample grid. For this experiment, 100 random sample locations were chosen and tested sequentially. Measurements were only made of the cuEN node for this test.

Fig. 8. Maps for cuGE node. The left maps show the excess (residual after trend is removed). The center maps show the re-trended signal map. The right maps show the residual kriging variance of the other maps.

When comparing those measurements to the predictions for the cuEN node, using the CINR metric alone, there is a Root Mean Square Error (RMSE) of 4.71, slightly higher than that found with cross validation, but still quite good overall.

F. Combining and Visualization

For coverage mapping, per-AP fitting is likely the best method, but in cognitive radio and interference detection applications it is necessary to create a composite map using data from many transmitters. This can be accomplished either by fitting and Kriging the entire set of measurements together

or by fitting and Kriging measurements from each transmitter separately and then combining the resulting maps. The first approach is the most conceptually straight forward, but has some problems. Combining measurements from multiple transmitters may produce a map with a large amount of per-location variation, possibly with colocated points of drastically varying value. Exactly colocated measurements of differing value can produce unsolvable Kriging equations and must be “jittered” to create a solvable equation with a unique solution. In the end, this approach can result in a map that is difficult to interpret and has a large error margin.

Due to the large variance at the same point due to different transmitters, the resulting map takes the form of a nearly constant value with peaks or holes centered at measurement locations. As a result, these data-combined maps do not provide information about the predicted coverage between points and are generally no more useful than simple color-coded dots located on a map. Given these concerns about this data combining method, we advocate an *ex post facto* combining which we will describe next.

Ex post facto map combining involves basic geospatial image tiling and combination. We use a basic two-pass method that first reads in all the map files to determine the total extent of the image, and then overlays the images, combining values at pixels as necessary. There are many ways we can combine maps this way, the most obvious is to take the maximum value for SNR-like metrics or the minimum value for EVM-like metrics. Figure 9 provides the combined maps for the CU WiMax measurements using these two combining methods. In the threshold-based combining, we count the number of transmitters whose interpolated signal is above 40 dB CINR⁷ (or below 60% in the case of the EVM metrics) and use this count (from 0 to 4) for the map. For the maximum-based combining, we actually use the minimum for the EVM metric, since a small value is good in this case. In a cognitive radio application, a threshold-based map like this could be used to locate contiguous regions where it is safe to transmit.

These maps make light of a few interesting observations. Firstly, the threshold maps make it plain to see regions and the contours between them where there is no coverage above the given threshold (light red) or substantial overlap (light green). Since two transmitters actually share the same frequency in this network, regions of light green might actually indicate potential for interference at the receiver. The maximum combining approach is less easy to interpret, but gives a complete picture of the propagation environment on the CU campus. For all metrics, there appears to be a coverage “hole” just west of the Gamow tower, located in the center of the map, which may indicate a misconfiguration in the downtilt of the west-pointing antennas for a building of this height (i.e., more downtilt might be necessary to avoid this hole). Additionally, the west-facing transmitters on the other tower, may fail to cover this region since the Gamow tower creates a shadow. Despite the seeming

⁷This threshold was empirically derived using a random (spatial) sample of upstream and downstream throughput measurements.

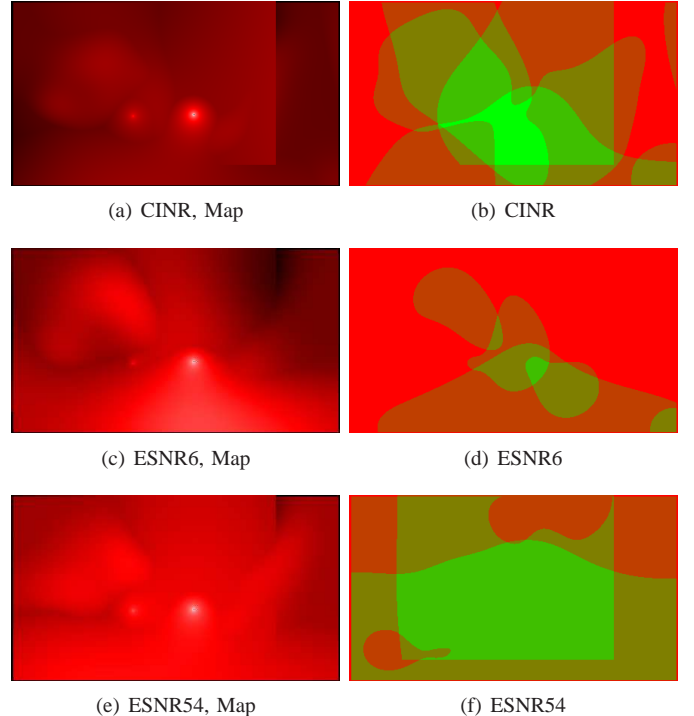


Fig. 9. Kriged maps for combined CU WiMax measurements using the CINR metric.

congruity of the maximum combined maps, the threshold maps reveal fairly disparate contours.

G. Small Scale Effects and Nonstationarity

In this section we want to understand how measurements vary over small time scales and small distances. An underlying assumption of the Kriging process is that the process being modeled is stationary, meaning that the (fitted) *mean* is constant in both time and space. Clearly, this is a strong assumption that the (often chaotic) radio environment is unlikely to obey. It is possible to loosen the stationarity assumption at the cost of substantial additional computational work, but in practice most users of Kriging processes opt to accept the implications of this assumption. By understanding how the radio environment changes over small time scales and small distances, we can put a bound on repeated measurement variation and hence a bound on the implicit unavoidable error associated with the stationarity assumption.

Fading in the radio environment can be classified into small-scale and large-scale fades. Large scale fades should be fairly constant over small distances and time, and hence are not troublesome—it is exactly the environment-specific large scale fading effects that our approach models. However, small-scale fades can be highly varying in time and over small distances because they stem from multipath effects and (possibly mobile) scatterers. As a practical rule of thumb many experimenters average measurements within 40 wavelengths (≈ 4.8 m) as a way to “average out” small scale effects [31]. In this section we seek to validate that standard practice as well as understand the scale of small scale effects over short

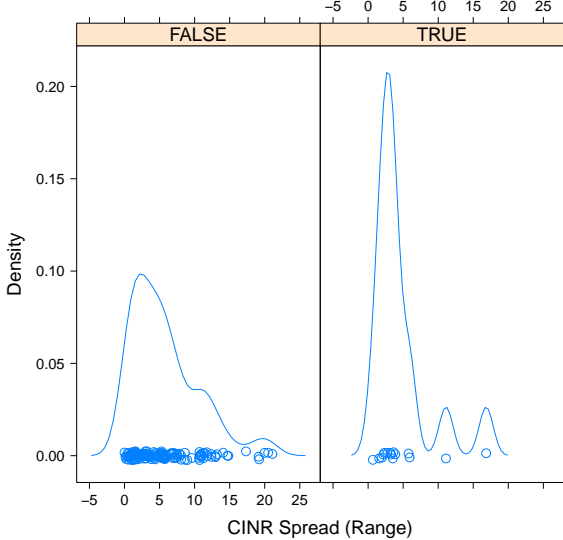


Fig. 10. Distribution of spread for measurements taken within 40 wavelengths (≈ 4.8 m) of each other (i.e., clustered/TRUE) versus at the same point at different times (i.e., unclustered/FALSE).

time scales.

After the initial University of Colorado at Boulder (CU) WiMax measurement campaign, a second campaign was undertaken to collect data at clustered locations so that the small scale (in space and time) variation can be compared to large scale trends. To this end, a random subset of approximately 15 grid points were selected and at each point, three complete measurements were taken at random locations within 40 wavelengths (≈ 4.8 m) of the original grid point. Figure 10 shows the amount of measurement spread observed at these closely clustered locations versus the amount of measurement spread between repeated measurements at the same location. Here, we use the nonparametric Median Absolute Deviation (MAD) as a measure of spread, although simple range (difference between largest and smallest observation) behaves similarly. Although the two distributions are not identical, they do appear to be Gaussian, with a similar central tendency and spread. Indeed, we have compared these distributions with a Welch two-sample t-test, two-sample Kolmogorov-Smirnov test, and Wilcoxon rank sum test (all of which test the null hypothesis that the difference in central tendency is significant), and none of the tests are willing to reject the null hypothesis that the data are drawn from the same distribution (p-values are between 0.3 and 0.5).

As an alternative view of this intrinsic channel variability, we look at the amount of variation observed between repeated measurements taken at the same location as a function of time. The amount of variation appears to be fairly stable for all of the metrics over small time scales (several minutes). There is a slight increase in measurement spread observed for the RCE and EVM measurements, but this does not appear to be substantial, and may not be significant. Interestingly, the ESNR metrics appear to have more intrinsic variation than the simpler

| Sampling | |
|-------------------------|------------------------------------------------------------------------------------------------|
| Initial Sampling Design | 100m Triangular Lattice with random clustered samples within 40 wavelengths (≈ 4.8 m) |
| Second Phase Sampling | None. A topic for <i>future work</i> . |
| Unreachable Points | Take measurement at nearest accessible location |
| Repeated Measurements | 1-3 per (regular or cluster) location to model small scale temporal variation |
| Postprocessing | |
| Null Measurements | Include with constant minimum value |
| Detrending | Subtract off Log/Log fit |
| The Variogram | |
| Variogram Fitting | Weighted Least Squares |
| Variogram Model | Gaussian or Cubic |
| Variogram Truncation | Necessary. 1000m performs well here. |
| Interpolation (Kriging) | |
| Method | Ordinary Kriging |
| Anisotropic Modeling | None. A topic for <i>future work</i> . |
| Nugget Tolerance | 0 |
| Prediction Resolution | 0.05 (low) - 0.2 (high) |

TABLE III
SUMMARY OF DERIVED BEST PRACTICES FOR GEOSTATISTICAL MAPPING OF WIRELESS NETWORK COVERAGE.

metrics which may be due to the fact that these metrics take into account more degrees of freedom (i.e., independent fading on each subcarrier).

Although it is likely that the radio environment is nonstationary at large time scales (days, weeks, and years), from these results it appears that the intrinsic variation is fairly stable on small time scales and hence repeated measurements are likely sufficient to characterize intrinsic variability. Because the geostatistical method explicitly models, rather than ignores, this intrinsic error, it can be treated as a feature of the resulting model instead of noise to be smoothed away. And, perhaps more importantly, by modeling the extent of small scale fading, we can put a lower bound on the achievable accuracy of *any* mapping campaign in a given environment, which helps quantify the obtainable fidelity of our model and also determine when sufficient measurements have been made.

V. CONCLUSION

In this paper, we have provided the first complete, real-world application of geostatistical modeling and interpolation to the problem of radio environment mapping. Although some other authors have proposed that geostatistical techniques may be appropriate for the domain, the work here is the first to actually apply the concepts and adapt them as necessary for the mapping of real transmitters. To analyze their efficacy, we have applied these techniques to the task of mapping the coverage and performance of a WiMax network in Boulder, Colorado. Table III provides a summary of the best practices derived from this investigation. Additionally, we have shown that this robust coverage map can be produced using a reasonably small amount of easily obtained data (several hundred samples on a hundred meter grid, for a space the size of a large university campus), which amounts to a tractable amount of routine “spade work” (approximately three days

work for a single dedicated experimenter). Automating this data collection will be an important step for the scalability of this approach, and we believe that there is much promise in research related to crowd-sourced data collection and in inexpensive commodity measurement devices. In forthcoming work, we have investigated the practicality of this approach as applied to large service areas, using less careful measurements (i.e., drive-test or crowd-sourced). Those results appear to suggest that geostatistical coverage mapping can be applied effectively and scaled naturally in those domains as well.

In general we see an error reduction of more than 10 dBs over common measurement-based methods and data-tuned *a priori* models when mapping CINR, and several dBs improvement with ESNR-based metrics. However, to focus only on the performance improvement is to miss the real value of the Kriging method. By implementing an appropriate sampling design, modeling the underlying spatial structure of the data, and using a statistical method we are able to generate an interpolated map with a well defined notion of residual error: the prediction at each point is a distribution, not simply a value. We investigated the scale of small scale fading (and hence deviation from stationarity) in the observations, and developed a method for combining observations from multiple BS measurement campaigns into one complete REM.

In future work, we will attempt to refine the models with additional “secondary” measurements that have been chosen to optimally reduce the residual error of the model. We have also begun to apply these methods to networks using different technologies and at different operating frequencies (2.4 GHz WiFi and 700 MHz LTE) with encouraging results. There are still important questions in terms of how measurement-based radio environment mapping can be automated and how models can be stored and queried efficiently. We offer the current work as a first attempt to demonstrate the core geostatistical techniques can be effectively and pragmatically applied in this domain and encourage researchers and commercial network operators to consider these powerful and statistically rigorous methods as a promising approach to the problem of empirical radio environment mapping.

REFERENCES

- [1] C. Phillips, D. Sicker, and D. Grunwald, “Bounding the error of path loss models,” in *IEEE Dynamic Spectrum Access Networks (DySPAN)*, May 2011.
- [2] R. Wahl, G. Wölfe, P. Wertz, P. Wildbolz, and F. Landstorfer, “Dominant path prediction model for urban scenarios,” in *14th IST Mobile and Wireless Communications Summit*, 2005.
- [3] J. Robinson, R. Swaminathan, and E. W. Knightly, “Assessment of urban-scale wireless networks with a small number of measurements,” in *MobiCom*, 2008.
- [4] A. Konak, “A kriging approach to predicting coverage in wireless networks,” *International Journal of Mobile Network Design and Innovation*, 2010.
- [5] M. Wellens, J. Riihijärvi, and P. Mähönen, “Spatial statistics and models of spectrum use,” *Comput. Commun.*, vol. 32, pp. 1998–2011, December 2009.
- [6] N. A. C. Cressie, *Statistics for Spatial Data*, revised ed. Wiley, 1993.
- [7] H. Wackernagel, *Multivariate Geostatistics*, 2nd ed., 1998, Ed. Springer.
- [8] M. Kanevski, Ed., *Advanced Mapping of Environmental Data*. ISTE Ltd. and John Wiley and Sons, Inc., 2008.
- [9] R. Olea, “Sampling design optimization for spatial functions,” *Mathematical Geology*, vol. 16, pp. 369–392, 1984.
- [10] E. A. Yfantis, G. T. Flatman, and J. V. Behar, “Efficiency of kriging estimation for square, triangular, and hexagonal grids,” *Mathematical Geology*, vol. 19, no. 3, pp. 183–205, 1987.
- [11] J. van Groenigen, W. Siderius, and A. Stein, “Constrained optimisation of soil sampling for minimisation of the kriging variance,” *Geoderma*, vol. 87, no. 3-4, pp. 239 – 259, 1999.
- [12] E. M. Delmelle and P. Goovaerts, “Second-phase sampling designs for non-stationary spatial variables,” *Geoderma*, vol. 153, pp. 205–216, 2009.
- [13] D. A. Cohn, Z. Ghahramani, and M. I. Jordan, “Active learning with statistical models,” *Journal of Artificial Intelligence Research*, vol. 4, pp. 129–145, 1996.
- [14] I. Staircase 3, “Open signal maps - cell phone tower and signal heat maps,” <http://opensignalmaps.com/>, October 2011.
- [15] K. Connelly, Y. Liu, D. Bulwinkle, A. Miller, and I. Bobbitt, “A toolkit for automatically constructing outdoor radio maps,” in *Proceedings of the International Conference on Information Technology: Coding and Computing (ITCC'05)*, vol. 2, apr. 2005, pp. 248 – 253 Vol. 2.
- [16] E. Dall’Anese, “Geostatistics-inspired sparsity-aware cooperative spectrum sensing for cognitive radio networks,” in *Proceedings of the Second International Workshop on Mobile Opportunistic Networking*, ser. MobiOpp ’10. New York, NY, USA: ACM, 2010, pp. 203–204.
- [17] A. Neskovic, N. Neskovic, and D. Paunovic, “Indoor electric field level prediction model based on the artificial neural networks,” *Communications Letters, IEEE*, vol. 4, no. 6, pp. 190 –192, Jun. 2000.
- [18] Y. Ould Isselmou, H. Wackernagel, W. Tabbara, and J. Wiart, “Geostatistical interpolation for mapping radio-electric exposure levels,” in *Antennas and Propagation, 2006. EuCAP 2006. First European Conference on*, 2006, pp. 1 – 6.
- [19] J. Riihijärvi, P. Mahonen, M. Wellens, and M. Gordziel, “Characterization and modelling of spectrum for dynamic spectrum access with spatial statistics and random fields,” in *Personal, Indoor and Mobile Radio Communications (PIMRC 2008)*, Sep 2008, pp. 1–6.
- [20] J. Riihijärvi, P. Mahonen, M. Petrova, and V. Kolar, “Enhancing cognitive radios with spatial statistics: From radio environment maps to topology engine,” in *CROWNCOM ’09*, June 2009, pp. 1 – 6.
- [21] J. Riihijärvi, P. Mahonen, and S. Sajjad, “Influence of transmitter configurations on spatial statistics of radio environment maps,” in *Personal, Indoor and Mobile Radio Communications*, Sep 2009, pp. 853 –857.
- [22] R. Olea, “A six-step practical approach to semivariogram modeling,” *Stochastic Environmental Research and Risk Assessment*, vol. 20, pp. 307–318, 2006.
- [23] X. Jian, R. A. Olea, and Y.-S. Yu, “Semivariogram modeling by weighted least squares,” *Computers & Geosciences*, vol. 22, no. 4, pp. 387 – 397, 1996.
- [24] P. J. R. Jr and P. J. Diggle, “geoR: a package for geostatistical analysis,” *R-NEWS*, vol. 1, no. 2, pp. 14–18, June 2001, iSSN 1609-3631.
- [25] C. Phillips and R. Senior, “CRAWDAD trace set pdx/metrofi,” Downloaded from <http://crawdad.cs.dartmouth.edu/pdx/metrofi>.
- [26] S. Rangarajan, “Geni - open, programmable wimax base station,” <http://www.winlab.rutgers.edu/docs/focus/GENI-WiMAX.html>, August 2011.
- [27] D. Halperin, W. Hu, A. Sheth, and D. Wetherall, “Predictable 802.11 packet delivery from wireless channel measurements,” in *ACM SIGCOMM*, 2010.
- [28] ———, “Tool release: gathering 802.11n traces with channel state information,” *SIGCOMM Computer Communications Review*, vol. 41, pp. 53–53.
- [29] S. Rayanchu, A. Patro, and S. Banerjee, “Airshark: Detecting non-wifi rf devices using commodity wifi hardware,” in *Internet Measurement Conference (IMC)*, November 2–4 2011.
- [30] D. Newbury and D. Bright, “Logarithmic 3-band color encoding: Robust method for display and comparison of compositional maps in electron probe x-ray microanalysis,” Surface and Microanalysis Science Division, National Institute of Standards and Technology (NIST), Tech. Rep., 1999.
- [31] W. C. Y. Lee, “Estimate of local average power of a mobile radio signal,” *IEEE Transactions on Vehicular Technology*, vol. VT-34, pp. 22–27, 1985.